



ELSEVIER

Contents lists available at ScienceDirect

## Journal of Sound and Vibration

journal homepage: [www.elsevier.com/locate/jsv](http://www.elsevier.com/locate/jsv)

# Broadband piezoelectric power generation on high-energy orbits of the bistable Duffing oscillator with electromechanical coupling

A. Erturk\*, D.J. Inman

Center for Intelligent Material Systems and Structures, Department of Mechanical Engineering, Virginia Polytechnic Institute and State University, Blacksburg, VA 24061, USA

## ARTICLE INFO

## Article history:

Received 5 July 2010

Received in revised form

13 October 2010

Accepted 15 November 2010

Handling Editor: K. Worden

Available online 13 December 2010

## ABSTRACT

An important issue in resonant vibration energy harvesters is that the best performance of the device is limited to a very narrow bandwidth around the fundamental resonance frequency. If the excitation frequency deviates slightly from the resonance condition, the power out is drastically reduced. In order to overcome this issue of the conventional resonant cantilever configuration, a non-resonant piezomagnetoelastic energy harvester has been introduced by the authors. This paper presents theoretical and experimental investigations of high-energy orbits in the piezomagnetoelastic energy harvester over a range of excitation frequencies. Lumped-parameter nonlinear equations (electromechanical form of the bistable Duffing oscillator with piezoelectric coupling) can successfully describe the large-amplitude broadband voltage response of the piezomagnetoelastic configuration. Following the comparison of the electromechanical trajectories obtained from the theory, it is experimentally verified that the piezomagnetoelastic configuration can generate an order of magnitude larger power compared to the commonly employed piezoelastic counterpart at several frequencies. Chaotic response of the piezomagnetoelastic configuration is also compared against the periodic response of the piezoelastic configuration theoretically and experimentally. Overcoming the bias caused by the gravity in vertical excitation of the piezomagnetoelastic energy harvester is discussed and utilization of high-energy orbits in the bistable structural configuration for electrostatic, electromagnetic and magnetostrictive transduction mechanisms is summarized.

© 2010 Elsevier Ltd. All rights reserved.

## 1. Introduction

The idea of harvesting ambient vibration energy to generate electricity has become a promising research field over the past decade due to the reduced power requirements of small electronic components. The motivation of vibration-based energy harvesting is to power such devices (e.g. sensor networks used in monitoring applications) by using the vibration energy available in their environment. Several researchers have reported their work on modeling and applications of vibration-based energy harvesting using electromagnetic [1,2], electrostatic [3,4], piezoelectric [5,6] and magnetostrictive [7,8] transduction mechanisms. Due to their large power densities, ease of application and feasibility of fabrication in micro-scale, piezoelectric energy harvesting has received the most attention [9–12].

Unless it is used as a surface patch, a piezo-stack or a cymbal arrangement, typically, a piezoelectric energy harvester is a cantilever with piezoceramic layers and it is located on a vibrating host structure for electrical power generation from

\* Corresponding author. Tel.: +1 540 231 0436; fax: +1 540 231 2903.

E-mail address: [erturk@vt.edu](mailto:erturk@vt.edu) (A. Erturk).

bending vibrations under resonance excitation. Such a design that operates effectively only at its linear resonance frequency is called a resonant energy harvester. Theoretical and experimental aspects of the linear cantilever design have been investigated extensively in the literature [5,6,13,14]. An important limitation of the commonly employed resonant energy harvester configuration is that the effective power generation performance of the device is limited to resonance excitation. If the excitation frequency deviates slightly from the fundamental resonance frequency of the energy harvester, the electrical power output is reduced by orders of magnitude. In order to overcome the bandwidth issue of the conventional cantilever configuration, researchers have considered utilizing some of the phenomena peculiar to nonlinear dynamical systems [15,16].

Implementation of the hardening stiffness in the (statically) monostable Duffing oscillator for increasing the frequency bandwidth was discussed by Burrow et al. [17] and Mann and Sims [18] for electromagnetic energy harvesting. Use of the hardening stiffness in the monostable form of the Duffing oscillator was also discussed by Ramlan et al. [19] along with snap-through in a bistable mass–spring–damper mechanism. More recently, the monostable Duffing oscillator with hardening stiffness was theoretically investigated by Daqaq [20] for random forcing. Bidirectional increase of the frequency bandwidth was studied by combining the softening and the hardening stiffness effects in the device proposed by Stanton et al. [21]. The bistable form of the Duffing oscillator was discussed by Cottone et al. [22] and Gammaitoni et al. [23] for noise excitation through the concept of stochastic resonance [24] as formerly pointed out by McInnes et al. [25] for energy harvesting. Stanton et al. [26] theoretically investigated the bifurcations of a bistable configuration similar to the one tested by Cottone et al. [22]. Another important aspect of the bistable Duffing oscillator has been pointed out by the authors [27] for piezoelectric energy harvesting using the well-known magnetoelastic structure [28]. Large-amplitude periodic oscillations on high-energy orbits of the bistable configuration have been shown to increase the open-circuit voltage output by a factor of three at several frequencies [27].

This work presents theoretical and experimental investigations of broadband high-energy orbits in a piezomagnetoelastic energy harvester along with a critique of the possible advantage of the chaotic response over the conventional periodic response. It is shown that lumped-parameter nonlinear equations (electromechanical form of the bistable Duffing oscillator with piezoelectric coupling) can successfully describe the broadband large-amplitude voltage response of the piezomagnetoelastic configuration. Electromechanical phase trajectories of the piezomagnetoelastic and the piezoelectric configurations are compared theoretically and the substantial advantage of the former is demonstrated. Following the theoretical simulations, it is experimentally verified that the *non-resonant* piezomagnetoelastic configuration can generate an order of magnitude larger power compared to the commonly employed *resonant* piezoelectric configuration at several frequencies. Chaotic response of the piezomagnetoelastic configuration is also compared against the periodic response of the piezoelectric configuration for the same base acceleration input. For vertical excitation of a horizontally located piezomagnetoelastic energy harvester, overcoming the bias caused by the gravity is discussed experimentally. Utilization of high-energy orbits in the bistable structural configuration for electrostatic, electromagnetic and magnetostrictive transduction mechanisms is addressed briefly.

## 2. Theoretical background and numerical simulations

### 2.1. Lumped-parameter electromechanical equations describing the nonlinear system dynamics

The magnetoelastic structure that forms the basis of this work was first investigated by Moon and Holmes [28] as a mechanical structure that exhibits strange attractor motions. The device consists of a ferromagnetic cantilever with two permanent magnets located symmetrically near the free end and it is subjected to harmonic base excitation. Depending on the magnet spacing, the ferromagnetic beam may have five (with three stable), three (with two stable) or one (stable) equilibrium positions since the bifurcations of the static problem are described by a butterfly catastrophe [29]. For the case with three equilibrium positions (statically bistable configuration), the governing lumped-parameter equation of motion for the fundamental vibration mode has the well-known form of the bistable Duffing equation [16,28,30], nonlinear dynamics of which was extensively analyzed by Holmes [30].

In order to use the magnetoelastic configuration as a piezoelectric energy harvester, we attached two piezoceramic layers onto the root of the cantilever and obtained a bimorph as depicted in Fig. 1 [27]. The piezoceramic layers are connected to a resistive electrical load and the voltage output across the load due to base excitation is of interest in energy harvesting. Introducing piezoelectric coupling into the bistable Duffing equation and applying the Kirchhoff laws to the circuit with a resistive load (Fig. 1) leads to the following electromechanical equations describing the nonlinear system dynamics for the fundamental vibration mode [27]<sup>1</sup>:

$$\ddot{x} + 2\zeta\dot{x} - \frac{1}{2}x(1-x^2) - \gamma v = f \cos \Omega t \quad (1)$$

$$\dot{v} + \lambda v + \kappa \dot{x} = 0 \quad (2)$$

<sup>1</sup> The factor 1/2 in front of the gradient of the dimensionless magnetoelastic energy ensures that the undamped ( $\zeta=0$ ) short-circuit ( $\lambda \rightarrow \infty$ , hence  $v \rightarrow 0$ ) natural frequency of small oscillations around either magnet is *unity* (which can be shown by substituting  $x = 1 + \bar{x}$  and linearizing in  $\bar{x}$ ). This is the convention preferred because the relevant phenomena discussed herein are mainly for excitation frequencies below this *post-buckled* natural frequency (thus for  $\Omega < 1$ ).

where  $x$  is the dimensionless tip displacement of the beam in the transverse direction,  $v$  is the dimensionless voltage across the load resistance,  $\zeta$  is the mechanical damping ratio,  $\Omega$  is the dimensionless excitation frequency,  $f$  is the dimensionless excitation force due to base acceleration ( $f \propto \Omega^2 X_0$ , where  $X_0$  is the dimensionless base displacement amplitude),  $\chi$  is the dimensionless piezoelectric coupling term in the mechanical equation,  $\kappa$  is the dimensionless piezoelectric coupling term in the electrical circuit equation,  $\lambda$  is the reciprocal of the dimensionless time constant ( $\lambda \propto 1/R_l C_p$ , where  $R_l$  is the load resistance and  $C_p$  is the equivalent capacitance of the piezoceramic layers) and an over-dot represents differentiation with respect to dimensionless time. The three static equilibrium positions obtained from Eq. (1) are  $(x, \dot{x}) = (0, 0)$  (a saddle) and  $(x, \dot{x}) = (\pm 1, 0)$  (two sinks). Note that the inherent piezoelectric nonlinearity [31–33] is ignored in Eqs. (1) and (2) by assuming the standard form of the linear piezoelectric constitutive relations [34].<sup>2</sup>

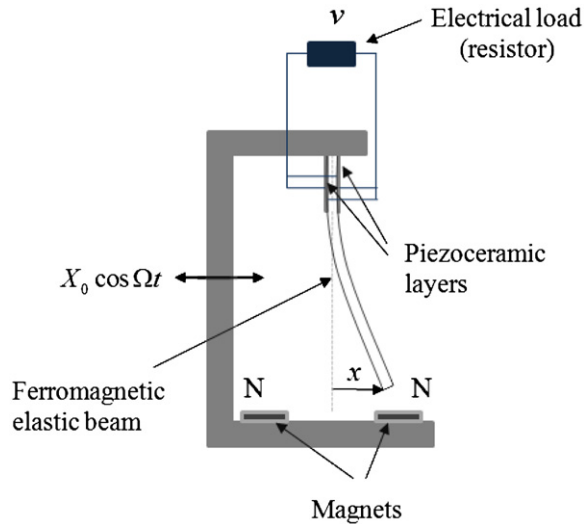


Fig. 1. Schematic of the piezomagnetoelastic energy harvester.

The state-space form of Eqs. (1) and (2) can be expressed as

$$\begin{Bmatrix} \dot{u}_1 \\ \dot{u}_2 \\ \dot{u}_3 \end{Bmatrix} = \begin{Bmatrix} u_2 \\ -2\zeta u_2 + \frac{1}{2} u_1 (1 - u_1^2) + \chi u_3 + f \cos \Omega t \\ -\lambda u_3 - \kappa u_2 \end{Bmatrix} \quad (3)$$

where the state variables are  $u_1 = x$ ,  $u_2 = \dot{x}$  and  $u_3 = v$ . The electromechanically coupled equations given by Eq. (3) can be used in an ordinary differential equation solver for numerical simulations (the *ode45* command of MATLAB is used here).

### 2.2. Time-domain numerical simulations of the electromechanical response

The time-domain voltage simulations shown in Figs. 2 and 3 are obtained using Eq. (3) with  $\Omega = 0.8$ ,  $\zeta = 0.01$ ,  $\chi = 0.05$ ,  $\kappa = 0.5$  and  $\lambda = 0.05$  (very close to open-circuit conditions). In the first case given by Fig. 2, the forcing term is  $f = 0.08$  and the motion starts with an initial deflection at one of the stable equilibrium positions ( $x(0) = 1$ ) with zero initial velocity and voltage ( $\dot{x}(0) = v(0) = 0$ ). The resulting vibratory motion is on a chaotic strange attractor, yielding the chaotic voltage history shown in Fig. 2a. The Poincaré map of this strange attractor motion is plotted on its phase portrait in Fig. 2b.

For the same system parameters and initial conditions, if the excitation amplitude is increased by 50% (to  $f = 0.12$ ), the transient chaotic response is followed by large-amplitude periodic oscillations on a high-energy orbit with substantially improved voltage response (Fig. 3a). Therefore, the attractor for this excitation amplitude is a large-amplitude periodic attractor, no longer a strange attractor. Remarkably, Fig. 3b shows that response on a very similar large-amplitude periodic attractor can be obtained for the original excitation amplitude ( $f = 0.08$ ) but different initial conditions (simply by imposing an initial velocity condition so that  $x(0) = 1$ ,  $\dot{x}(0) = 1.3$ ,  $v(0) = 0$ ).<sup>3</sup> This second case corresponds to the coexistence of a strange

<sup>2</sup> It is worth adding that piezoelectric coupling in the mechanical equation is a relatively *weak* coupling effect (on the order of mechanical damping) while the nonlinearity caused by the bistability is *strong*. Therefore, the feedback sent from the electrical domain to the mechanical domain due to Joule heating in the resistor or due to more sophisticated harvesting circuits [35–40] is not expected to suppress the resulting strongly nonlinear phenomena discussed in this paper. The former is shown experimentally in Section 3.5 for the resistor sweep.

<sup>3</sup> Lyapunov functions showing the stability of these limit-cycles obtained under large forcing (as well as the stability of the limit-cycles around the focus points for small forcing) are given by Holmes [30]. The presence of piezoelectric coupling with an external resistor does not alter the positive definiteness of the Lyapunov function nor does it alter the negative definiteness of its time derivative.

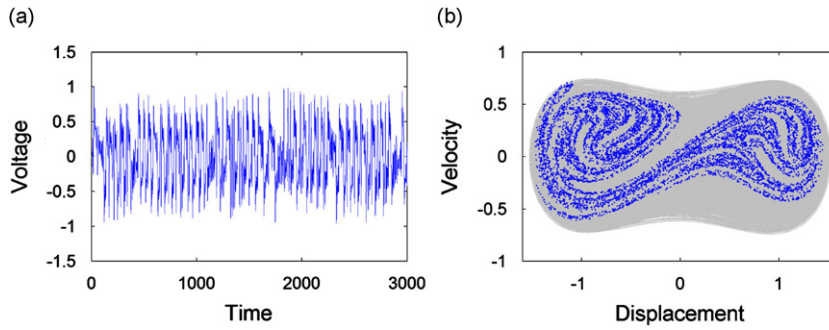


**Fig. 2.** (a) Theoretical voltage history obtained from the strange attractor motion and (b) the Poincaré map of the motion on its phase portrait ( $x(0)=1$ ,  $\dot{x}(0)=0$ ,  $v(0)=0$ ,  $f=0.08$ ,  $\Omega=0.8$ ).

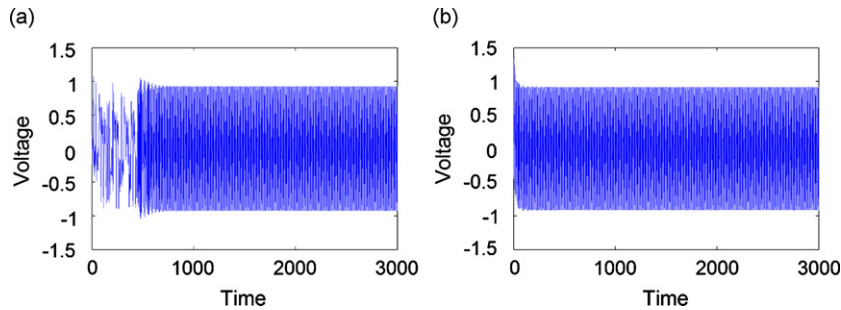


**Fig. 3.** Theoretical voltage histories: (a) large-amplitude response due to the excitation amplitude ( $x(0)=1$ ,  $\dot{x}(0)=0$ ,  $v(0)=0$ ,  $f=0.12$ ,  $\Omega=0.8$ ) and (b) large-amplitude response due to the initial conditions for a lower excitation amplitude ( $x(0)=1$ ,  $\dot{x}(0)=1.3$ ,  $v(0)=0$ ,  $f=0.08$ ,  $\Omega=0.8$ ).

attractor with a large-amplitude periodic attractor for the same forcing level as formerly discussed by Guckenheimer and Holmes [16]. Hence, for the same amount of forcing, depending on the initial conditions, the system can be attracted by the high-energy periodic orbit (Fig. 3b) instead of the strange attractor (Fig. 2a). Obviously the large-amplitude periodic orbit is preferred for energy harvesting and therefore the focus is mainly placed on the response form of Fig. 3b in this paper.

### 2.3. Performance comparison of the piezomagnetoelastic and the piezoelastic configurations in the phase space

Having observed the large-amplitude electromechanical response of the piezomagnetoelastic energy harvester configuration described by Eq. (3), comparisons can be made against the conventional piezoelastic configuration (i.e. the commonly employed [5,6,9–14] cantilever configuration without the magnets causing the bistability).

The lumped-parameter electromechanical equations of the linear piezoelastic configuration for the fundamental vibration mode are<sup>4</sup>

$$\ddot{x} + 2\zeta\dot{x} + \frac{1}{2}x - \chi v = f \cos \Omega t \quad (4)$$

$$\dot{v} + \lambda v + \kappa \dot{x} = 0 \quad (5)$$

which can be given in the state-space form as

$$\begin{Bmatrix} \dot{u}_1 \\ \dot{u}_2 \\ \dot{u}_3 \end{Bmatrix} = \begin{Bmatrix} u_2 \\ -2\zeta u_2 - \frac{1}{2}u_1 + \chi u_3 + f \cos \Omega t \\ -\lambda u_3 - \kappa u_2 \end{Bmatrix} \quad (6)$$

where the state variables are as defined previously. For the same system parameters ( $\Omega=0.8$ ,  $\zeta=0.01$ ,  $\chi=0.05$ ,  $\kappa=0.5$  and  $\lambda=0.05$ ), initial conditions and the forcing amplitude of Fig. 3b ( $x(0)=1$ ,  $\dot{x}(0)=1.3$ ,  $v(0)=0$ ,  $f=0.08$ ), one can simulate the voltage response of the piezoelastic configuration using Eq. (6).

<sup>4</sup> The factor 1/2 is preserved in Eq. (4) so the undamped short-circuit natural frequency of the piezoelastic configuration is  $1/\sqrt{2}$  (hence the theoretical discussion is close to the experimental setup discussed in this paper). It will be seen in Section 3 that the fundamental post-buckled resonance frequency of the piezomagnetoelastic configuration is 10.6 Hz whereas the fundamental resonance frequency of the piezoelastic configuration is 7.4 Hz (these are roughly proportional to 1 and  $1/\sqrt{2}$  obtained from Eqs. (1) and (4), respectively).

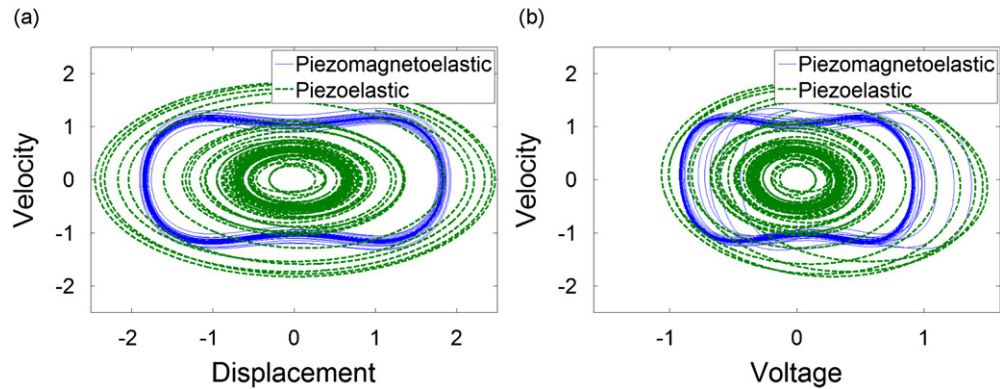


**Fig. 4.** Comparison of the (a) velocity vs. displacement and the (b) velocity vs. open-circuit voltage phase portraits of the piezomagnetoelastic and the piezoelastic configurations ( $x(0)=1$ ,  $\dot{x}(0)=1.3$ ,  $v(0)=0$ ,  $f=0.08$ ,  $\Omega=0.8$ ).

Fig. 4a shows the velocity vs. displacement trajectories of the piezomagnetoelastic and the piezoelastic configurations. As can be seen from the periodic orbits appearing in this figure, for the same excitation amplitude, system parameters and the forcing amplitude, the steady-state vibration amplitude of the piezomagnetoelastic configuration can be much larger than that of the piezoelastic configuration. Expectedly, the large-amplitude periodic (limit-cycle) response on the high-energy orbit of the piezomagnetoelastic configuration is also observed in the velocity vs. voltage trajectory shown in Fig. 4b.<sup>5</sup>

The advantage of the piezomagnetoelastic configuration over the piezoelastic configuration can be shown by plotting these trajectories at several other frequencies. The three-dimensional voltage vs. velocity trajectories are given for the frequency range of  $\Omega=0.5-1$  in Fig. 5. In all cases, the system parameters, initial conditions and the forcing amplitude<sup>6</sup> are the identical. In Fig. 5a ( $\Omega=0.5$ ), the electrical output of the piezomagnetoelastic configuration is not considerably larger because the elastic beam oscillates around  $x(0)=1$  (small-amplitude limit-cycle [16,30]). That is, the forcing amplitude is insufficient to overcome the attraction of the magnetic force at the respective focus. As a result, the piezomagnetoelastic configuration oscillates on a low-energy orbit and its electrical response amplitude is indeed comparable to that of the piezoelastic configuration. In Fig. 5b, d–f (for  $\Omega=0.6, 0.8, 0.9$  and  $1$ ), however, the piezomagnetoelastic configuration shows very large amplitude electromechanical response on high-energy orbits compared to the orbits of the piezoelastic configuration. Only near the resonance frequency of the piezoelastic configuration, the response amplitude of the piezoelastic configuration is larger (Fig. 5c). Nevertheless, at this particular frequency where the resonant configuration generates more voltage, the difference in the response amplitudes is not as dramatic as at other frequencies where the non-resonant configuration is superior.<sup>7</sup>

#### 2.4. Comparison of the chaotic response and the large-amplitude periodic response

As mentioned previously, large-amplitude attracting orbits of the piezomagnetoelastic configuration might coexist with strange attractors [16,30]. The advantage of the large-amplitude periodic response of the piezomagnetoelastic configuration shown in Fig. 3b over the piezoelastic configuration is evident in Figs. 4 and 5d. If the initial velocity condition is removed, it is known from Fig. 2 that the response will be on a strange attractor. It is worth comparing the chaotic response in the piezomagnetoelastic configuration with the periodic response in the piezoelastic configuration (for  $x(0)=1$ ,  $\dot{x}(0)=0$ ,  $v(0)=0$ ,  $f=0.08$ ,  $\Omega=0.8$ ). For the time interval shown in Fig. 6a, the chaotic response in the piezomagnetoelastic configuration generates 46.5% larger root mean square (rms) voltage than the periodic response of the conventional piezoelastic configuration. When the initial velocity condition ( $\dot{x}(0)=1.3$ ) is imposed to catch the large-amplitude orbit (as in Fig. 3b), the rms voltage output of the piezomagnetoelastic configuration is 113.7% larger than that of the conventional piezoelastic configuration for the same time interval (Fig. 6b). Note that the only difference between the simulations in Fig. 6a and b is the initial velocity condition, which strongly affects the form of the steady-state response in the piezomagnetoelastic

<sup>5</sup> For the system parameters used in these simulations, the system is very close to open-circuit conditions and the phase between the voltage and the velocity is approximately  $90^\circ$ . Therefore, in open-circuit conditions, it is reasonable to plot the velocity vs. voltage output as the *electromechanical phase portrait* (as an alternative to the conventional velocity vs. displacement phase portrait). From the experimental point of view, it is advantageous to plot these two independent measurements (voltage output of the piezoceramic vs. the velocity signal from the laser vibrometer) instead of integrating the experimental velocity history (which often results in a non-uniform drift).

<sup>6</sup> The forcing amplitude in the base excitation problem is proportional to the square of the frequency ( $f \propto \Omega^2 X_0$ ) [6,13,14]. Keeping the forcing amplitude  $f$  constant at different frequencies implies keeping the base acceleration amplitude the same. Hence the base displacement amplitudes are different.

<sup>7</sup> Note that the comparisons in Figs. 4 and 5 are for the open-circuit voltage output (not for an arbitrary electrical load). Although comparing the optimum power values would be more precise, both the piezoelastic and the piezomagnetoelastic configurations have the same piezoelectric coupling, capacitance and mechanical damping (and the frequencies of interest are identical). Therefore the configurations are not expected to have substantially different (i.e. several orders of magnitude different) matched resistance values. This assumption is verified experimentally in the power output comparisons of Section 3.5.

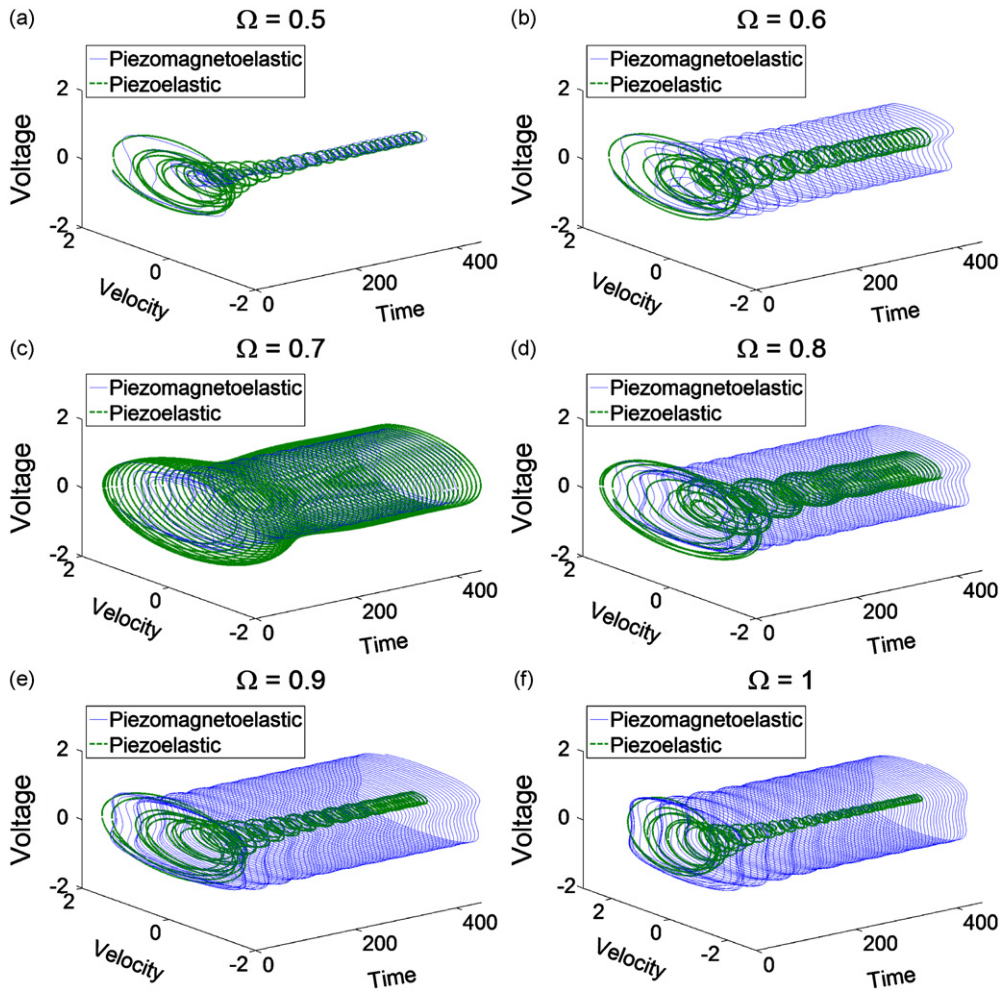


**Fig. 5.** Comparison of the open-circuit voltage vs. velocity phase trajectories of the piezomagnetoelastic and the piezoelectric configurations for (a)  $\Omega=0.5$ , (b)  $\Omega=0.6$ , (c)  $\Omega=0.7$ , (d)  $\Omega=0.8$ , (e)  $\Omega=0.9$ , and (f)  $\Omega=1$  ( $x(0)=1, \dot{x}(0)=1.3, v(0)=0, f=0.08$ ).

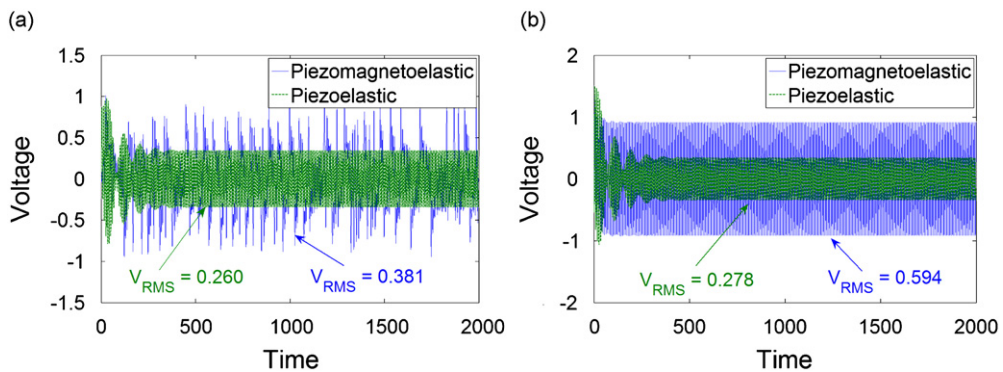


**Fig. 6.** Comparisons of (a) the chaotic response in the piezomagnetoelastic configuration ( $x(0)=1, \dot{x}(0)=0, v(0)=0, f=0.08, \Omega=0.8$ ) and (b) the large-amplitude periodic response in the piezomagnetoelastic configuration ( $x(0)=1, \dot{x}(0)=1.3, v(0)=0, f=0.08, \Omega=0.8$ ) against the piezoelectric configuration close to open-circuit conditions.

configuration. The large-amplitude periodic response of the piezomagnetoelastic configuration is preferred to chaos not just because of its 2.5 times larger voltage gain compared to that of the chaotic response but also because the periodic response is preferred to chaotic response when designing a nonlinear energy harvesting circuit in order to charge a battery or a capacitor efficiently [35–40].

### 3. Experimental verifications

#### 3.1. Experimental setup

Fig. 7a shows the piezomagnetoelastic energy harvester and the setup used for the experimental verifications. Close-up views of the piezomagnetoelastic configuration (elastic cantilever with the magnets causing the bistability) and the piezoelastic configuration (conventional elastic cantilever obtained when the magnets are removed) are shown in Figs. 7b and c, respectively. Harmonic base excitation is provided by a seismic shaker (Acoustic Power Systems APS-113), the acceleration at the base of the cantilever is measured by a small accelerometer (PCB Piezotronics U352C67) and the velocity response of the cantilever is recorded by a laser vibrometer (Polytec PDV-100). The time history of the base acceleration, voltage and vibration responses are recorded by a National Instruments NI-cDAQ data acquisition system (with a sampling frequency of 2000 Hz). The ferromagnetic beam is made of tempered blue steel and it is 145 mm long (overhang length), 26 mm wide and 0.26 mm thick. A lumped mass of 14 g is attached close to the tip for improved dynamic flexibility. Two PZT-5A piezoceramic layers (Midé Corporation QP16N) are attached onto both faces of the beam at the root using a high-shear strength epoxy and their electrodes are connected in parallel. The center-to-center spacing between the symmetrically located circular rare earth magnets is 50 mm and this distance is selected to realize the three equilibrium case described by Eq. (1). The tip deflection of the magnetically buckled beam in the static case to either side is approximately 15 mm relative to the statically unstable equilibrium position. The fundamental post-buckled resonance frequency of the beam is 10.6 Hz (for small oscillations around each magnet) whereas the fundamental resonance frequency of the unbuckled beam (when the magnets are removed) is 7.4 Hz (both under the open-circuit conditions of piezoceramics, i.e. at constant electric displacement). Before the comparison of the piezomagnetoelastic (Fig. 7b) and the piezoelastic (Fig. 7c) configurations, the individual performance results of the piezomagnetoelastic configuration [27] are reviewed for the sake of completeness.

#### 3.2. Performance results of the piezomagnetoelastic configuration

For a base acceleration amplitude of 0.5g (where  $g$  is the gravitational acceleration:  $g=9.81 \text{ m/s}^2$ ) at 8 Hz, with an initial deflection at one of the stable equilibrium positions (15 mm to the shaker side), zero initial velocity and voltage, the chaotic open-circuit voltage response shown in Fig. 8a is obtained [27]. The Poincaré map of the strange attractor motion is displayed

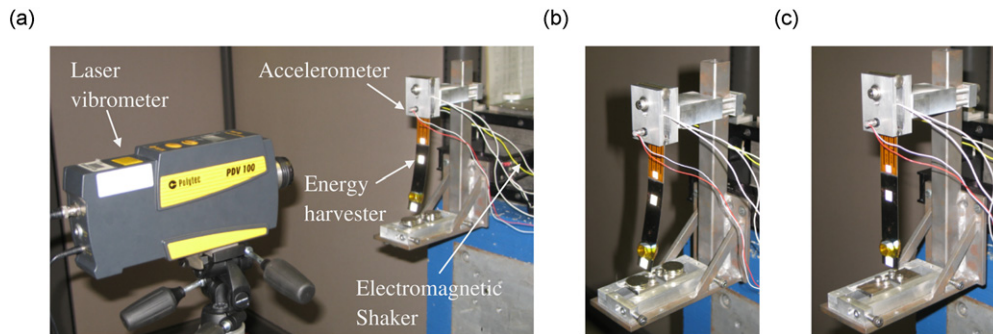


Fig. 7. (a) Experimental setup with the piezoelectric energy harvester, seismic shaker, accelerometer and laser vibrometer, (b) piezomagnetoelastic configuration, and (c) piezoelastic configuration.

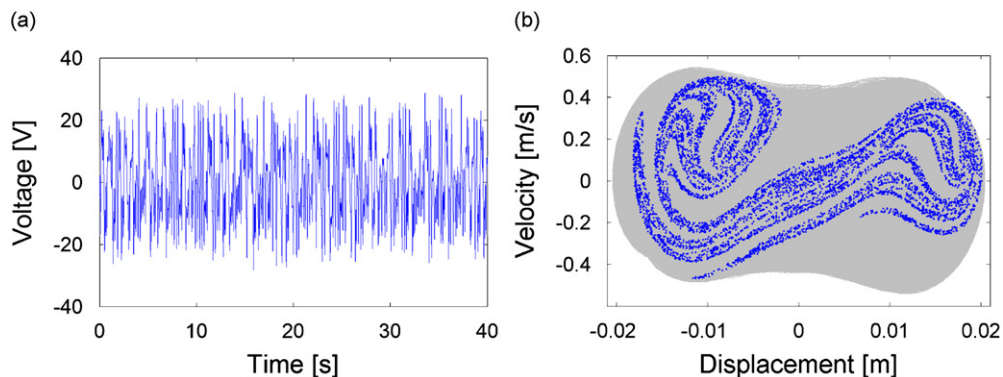
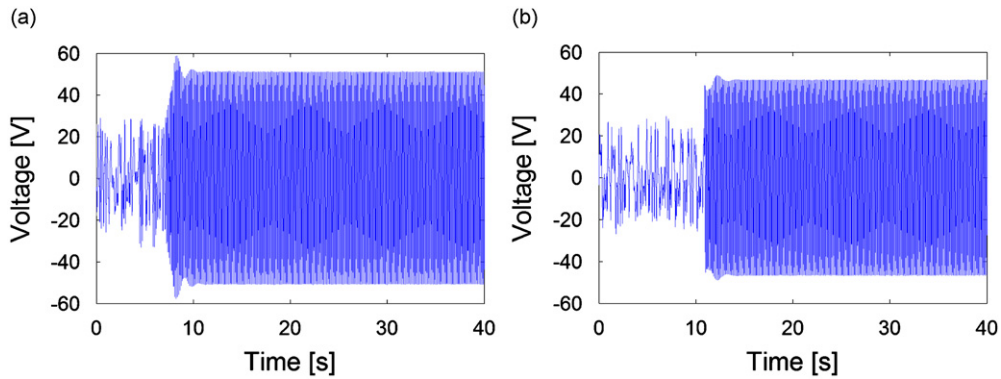
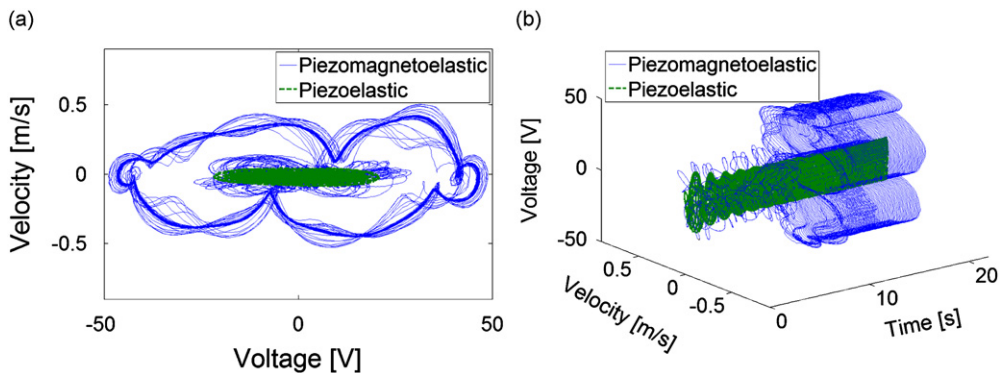


Fig. 8. (a) Experimental open-circuit voltage history obtained from the strange attractor motion and (b) the Poincaré map of the motion on its phase portrait (excitation: 0.5g at 8 Hz).



**Fig. 9.** Experimental open-circuit voltage histories: (a) large-amplitude response due to the excitation amplitude (excitation: 0.8g at 8 Hz) and (b) large-amplitude response due to a disturbance at  $t=11$  s for a lower excitation amplitude (excitation: 0.5g at 8 Hz)



**Fig. 10.** (a) Two-dimensional and (b) three-dimensional comparisons of the electromechanical trajectories in the piezomagnetoelastic and the piezoelectric configurations (excitation: 0.5g at 8 Hz with a disturbance at  $t=11$  s).

in Fig. 8b on its phase portrait. These figures are obtained from a measurement taken for about 15 min (1,784,400 data points due to a sampling frequency of 2000 Hz) and they exhibit very good qualitative agreement with the numerical simulations given in Fig. 2.

For the same initial conditions, if the excitation amplitude is increased to 0.8g (similar to the amount of increase in the theoretical simulation) by keeping the frequency the same, the response turns from transient chaos into a large-amplitude periodic motion with a strong improvement in the open-circuit voltage response as shown in Fig. 9a (analogous to Fig. 3a). Therefore, the strange attractor of Fig. 8a is replaced by a large-amplitude periodic attractor in Fig. 9a due to the increased forcing amplitude. A similar improvement is obtained in Fig. 9b, where the excitation amplitude is kept as the original one (0.5g) and a disturbance (hand impulse) is applied at  $t=11$  s (as a simple alternative to creating an initial velocity condition, analogous to Fig. 3b).<sup>8</sup> This second case corresponds to coexistence of a strange attractor and a large-amplitude periodic attractor for the same level of forcing [16,30]. Therefore, the system stays on the strange attractor (Fig. 8a) in the absence of any disturbance and the aforementioned disturbance results in a large-amplitude periodic response (Fig. 9b) with a substantial energy gain as discussed in the following. These experimental results (Fig. 9) exhibit good agreement with the theoretical discussion (Fig. 3). The next step is to compare the piezomagnetoelastic and the piezoelectric configurations experimentally.

### 3.3. Comparison of the piezomagnetoelastic and the piezoelectric configurations for voltage generation

Fig. 10a compares the velocity vs. open-circuit voltage trajectories of the piezomagnetoelastic and the piezoelectric configurations for a base excitation amplitude of 0.5g at 8 Hz. The chaotic part of response in the piezomagnetoelastic configuration belongs to the time interval before the disturbance is applied. This figure is therefore analogous to the

<sup>8</sup> In practice, such a disturbance (an impulse) can be realized by an electromagnet (or by one of the piezoceramic patches) initially and its power requirement can be compensated for by harvesting energy for a sufficiently long time.

<sup>9</sup> In the experiments, the piezoelectric configuration is obtained simply by removing the magnets of the piezomagnetoelastic configuration after the experiments of the latter are completed.

theoretical demonstration given by Fig. 4b. The three-dimensional view of the electromechanical trajectory in the electromechanical phase space is shown in Fig. 10b and it exhibits good qualitative agreement with its simplified theoretical counterpart based on lumped-parameter modeling (e.g. Fig. 5d).

### 3.4. On the chaotic and the large-amplitude periodic regions of the response

Before the broadband comparisons of the piezomagnetoelastic and the piezoelectric configurations, the voltage history of Fig. 10b is reconsidered in two parts. The time history until the instant of the disturbance is chaotic, which would yield a strange attractor motion similar to Fig. 8 if no disturbance was applied. After the disturbance is applied at  $t=11$  s, the large-amplitude response on a high-energy orbit is obtained. In order to visualize the advantage of the second region in the response history of Fig. 10b, the open-circuit voltage histories of the piezomagnetoelastic and the piezoelectric configurations are compared for the same harmonic input (0.5g at 8 Hz). The acceleration inputs to the piezomagnetoelastic and the piezoelectric configurations at an arbitrary instant of time are shown in Fig. 11a. The voltage input to the seismic shaker is identical for both configurations, yielding very similar base acceleration amplitudes for a fair comparison. Fig. 11b displays the comparison of the piezomagnetoelastic and the piezoelectric configurations, where the former exhibits chaotic response while the latter has already reached its periodic steady-state response at the input frequency. As a rough comparison, from Fig. 11b, it is not possible to claim that the chaotic response of the piezomagnetoelastic configuration has any substantial advantage over the harmonic response of the piezoelectric configuration as their amplitudes look very similar (this is further discussed in the following paragraph). Fig. 11c shows the voltage histories of these configurations some time after the disturbance is applied to the piezomagnetoelastic configuration and the large-amplitude periodic response is obtained. Obviously, if the same disturbance is applied to the piezoelectric configuration, the trajectory (in the phase space) returns to the same low-energy orbit after some transients since no such high-energy attractor exists in the piezoelectric configuration. Therefore, the response amplitude of the piezoelectric configuration is identical in Fig. 11b and c. However, the large-amplitude response of the piezomagnetoelastic configuration can give more than three times larger rms voltage output according to Fig. 11c.

In order to verify the claim that the chaotic response region of the piezomagnetoelastic configuration may not have a substantial advantage over to the periodic response of the piezoelectric configuration, the time histories of both configurations are compared in the absence of any disturbance (so the piezomagnetoelastic configuration stays on a strange attractor as in Fig. 8 instead of being attracted by the high-energy orbit as in Fig. 10). For a base acceleration amplitude of 0.5g at 8 Hz, the

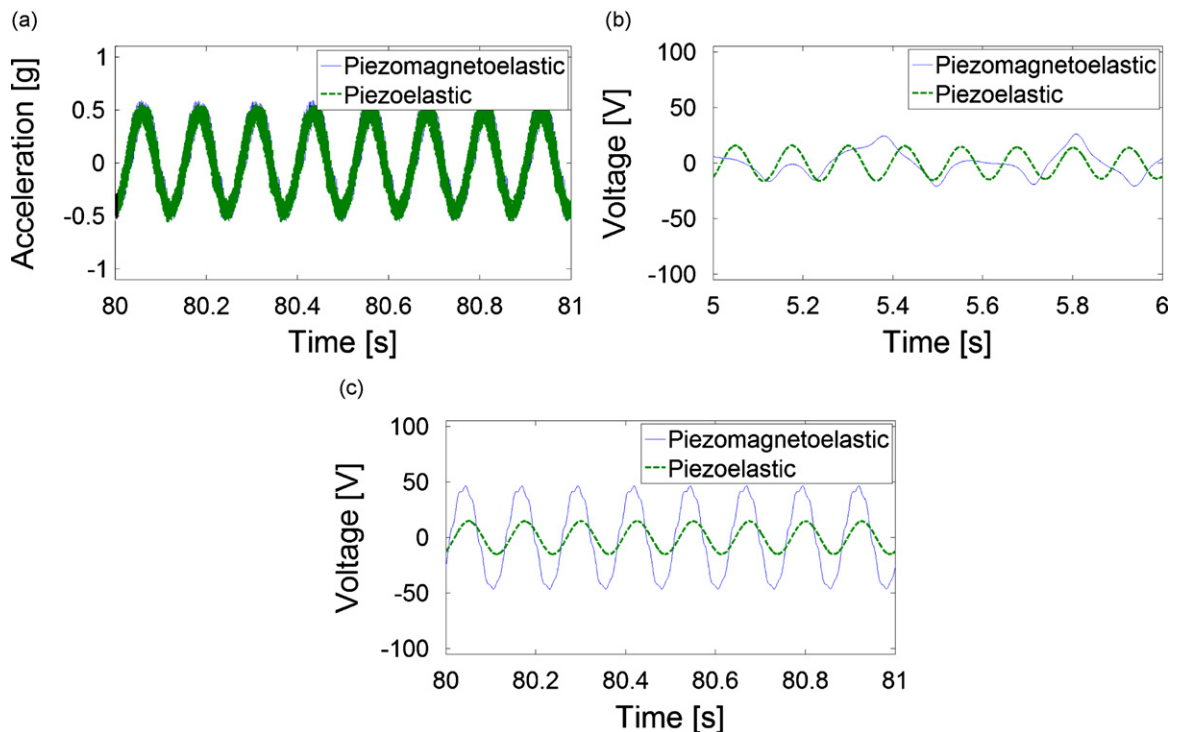


**Fig. 11.** Comparison of the input and the output time histories of the piezomagnetoelastic and piezoelectric configurations: (a) input acceleration histories, (b) open-circuit voltage outputs in the chaotic response region of the piezomagnetoelastic configuration, and (c) open-circuit voltage outputs in the large-amplitude periodic response region of the piezomagnetoelastic configuration (excitation: 0.5g at 8 Hz with a disturbance at  $t=11$  s).

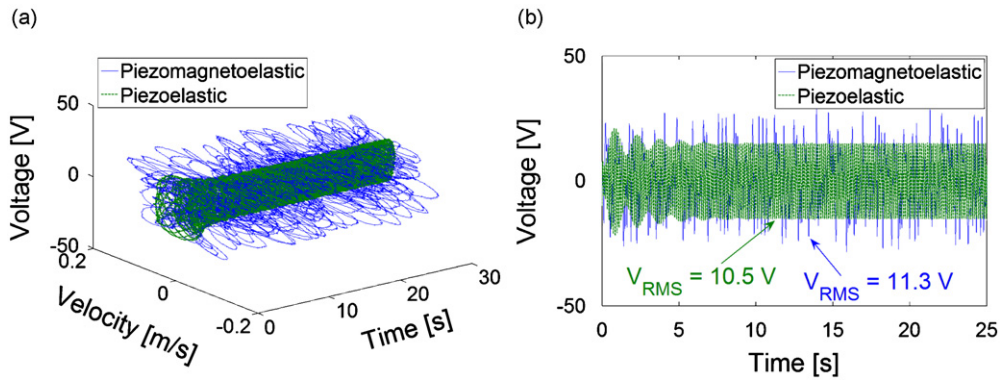


**Fig. 12.** Comparison of the chaotic response in the piezomagnetoelastic configuration and the periodic response in the piezoelectric configuration (excitation: 0.5g at 8 Hz, no disturbance is applied): (a) voltage vs. velocity trajectory and (b) voltage history showing the rms values.

electromechanical trajectories of the piezomagnetoelastic and the piezoelectric configurations are shown in Fig. 12a. The three-dimensional chaotic trajectory of the piezomagnetoelastic configuration shows larger instantaneous voltage and velocity amplitudes in Fig. 12a. However, as shown in Fig. 12b, the rms voltage output of the piezomagnetoelastic configuration (obtained for the interval of 0–25 s) is only 7.6% larger than that of the piezoelectric configuration (it is observed that these rms values do not change considerably with increasing time interval). Consequently, no substantial improvement is obtained in the chaotic response region. Moreover, one would prefer a periodic signal to a chaotic signal for designing an efficient energy harvesting circuit for storage applications [35–40]. Along with the theoretical discussion given in Section 2.4, this observation justifies our efforts of focusing on the large-amplitude periodic oscillations rather than chaos in the bistable structure. Broadband power generation performance results of both configurations are presented next.

### 3.5. Broadband performance comparison

Harmonic base excitation of 0.5g amplitude (yielding an rms value of approximately 0.35g) is applied at frequencies of 5, 6, 7 and 8 Hz. Fig. 13 shows the comparison of the average steady-state power vs. load resistance graphs of the piezomagnetoelastic and the piezoelectric configurations at these frequencies. Note that the excitation amplitudes of both configurations are very similar in all cases. The piezomagnetoelastic energy harvester gives an order of magnitude larger power at 5, 6 and 8 Hz while the piezoelectric configuration gives larger power only at 7 Hz (by a factor of 2.3), which is close to its resonance frequency.<sup>10</sup> The average power outputs read from these graphs for the optimum values of load resistance are listed in Table 1. Note that the electrical resistance values resulting in the maximum power output do not suppress the strongly nonlinear phenomena discussed herein, i.e. the shunt damping effect of piezoelectric power generation on the large-amplitude limit cycles is negligible (which is observed experimentally from the velocity response).

Not all the response forms in the piezomagnetoelastic configuration start with chaotic motion. For instance, for excitation at 6 Hz, the motion of the piezomagnetoelastic configuration starts with small-amplitude limit-cycle oscillations around one of the focus points. The disturbance applied at  $t=11$  s results in large-amplitude limit-cycle oscillations as summarized in Fig. 14. Therefore, not only chaotic vibrations but also small-amplitude limit-cycle oscillations around one of the magnets can be turned into large-amplitude limit-cycle oscillations.

Variations of the average electrical power outputs of both configurations with the excitation frequency are plotted in Fig. 15. It is important to notice in this figure is that, at several frequencies, the non-resonant piezomagnetoelastic energy harvester can indeed generate one order of magnitude more power for the same input. The resonant piezoelectric energy harvester can generate larger power only within a narrow band around its fundamental resonance frequency. However, this power output is not an order of magnitude larger than that of the piezomagnetoelastic configuration (in qualitative agreement with Fig. 5c). It can be concluded that the piezomagnetoelastic configuration exhibits substantially better broadband power generation performance provided that the input excitation results in oscillations on its high-energy orbits in the frequency range of interest. Given the frequency range and the amplitude of harmonic base excitation at these frequencies, the piezomagnetoelastic energy harvester should be designed to be attracted by these high-energy orbits.<sup>11</sup>

<sup>10</sup> For the same excitation amplitude, the piezomagnetoelastic configuration cannot escape the attraction of the low-energy orbit when excited at 4 Hz (analogous to the theoretical case in Fig. 5a) whereas the attractor is chaotic at 9 Hz.

<sup>11</sup> It is worth mentioning that, like several other bistable systems, the piezomagnetoelastic energy harvester exhibits *stochastic resonance* [22–25] under noise excitation provided that a certain threshold of input variance is exceeded. Recently, Litak et al. [41] used Eqs. (1) and (2) given by Erturk et al. [27] and showed the stochastic resonance in the electrical response to Gaussian white noise input.

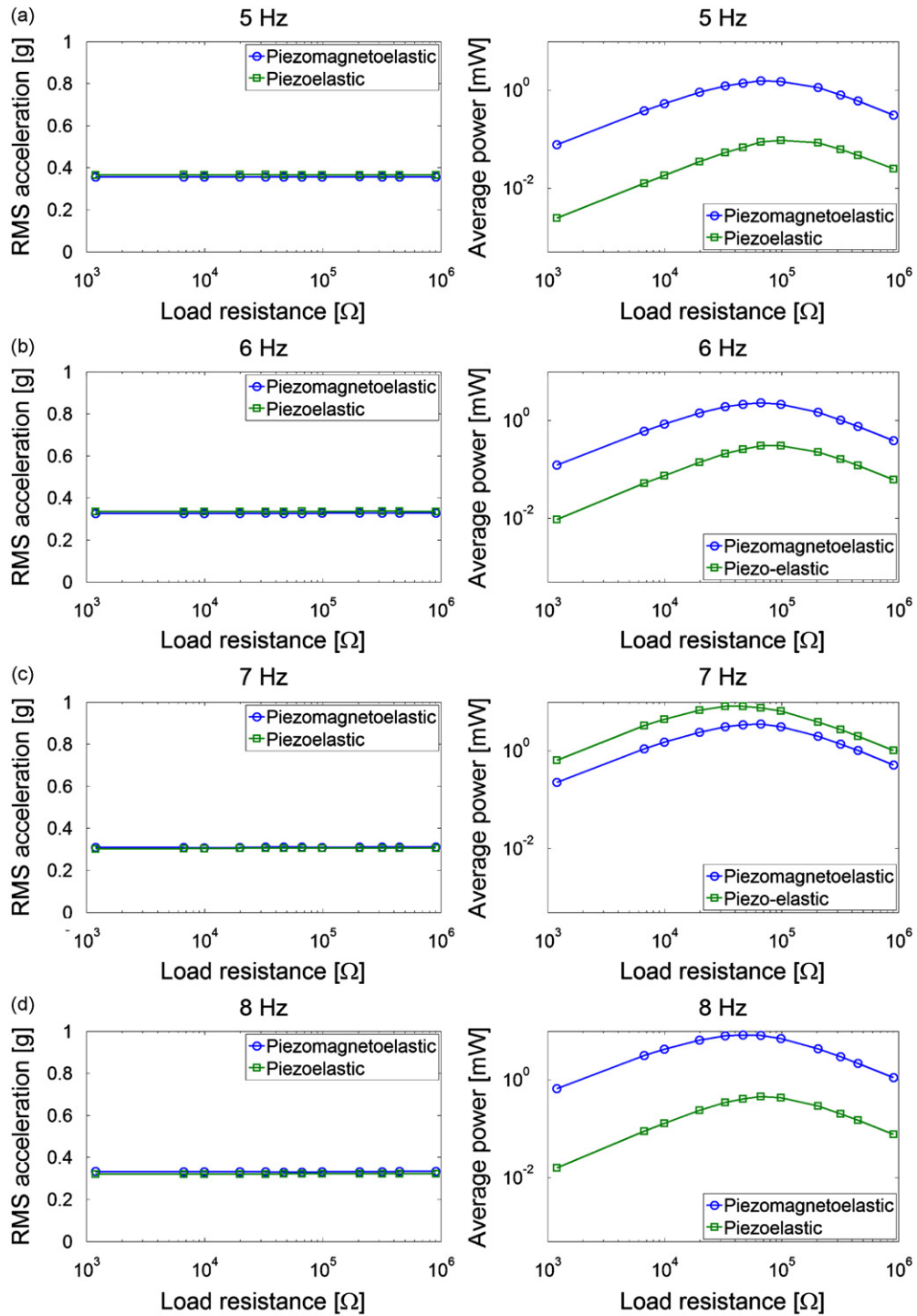


Fig. 13. Comparison of the acceleration inputs and power outputs of the piezomagnetoelastic and the piezoelastic configurations at steady state for a range of excitation frequencies: (a) 5 Hz, (b) 6 Hz, (c) 7 Hz, and (d) 8 Hz.

#### 4. Vertical excitation of the piezomagnetoelastic energy harvester

In physical applications, the direction of vibratory motion is often vertical as depicted in Fig. 16. In such a case, the gravitational force field might distort the static equilibrium of the flexible cantilever considerably, which might affect the condition of static bistability. The sag of the elastic beam due to its own weight can cause the beam to become biased toward

**Table 1**

Comparison of the average power outputs of the piezomagnetoelastic and piezoelectric energy harvester configurations (rms acceleration input: 0.35g).

Excitation frequency (Hz)	5	6	7	8
Piezomagnetoelastic configuration (mW)	1.57	2.33	3.54	8.45
Piezoelectric configuration (mW)	0.10	0.31	8.23	0.46

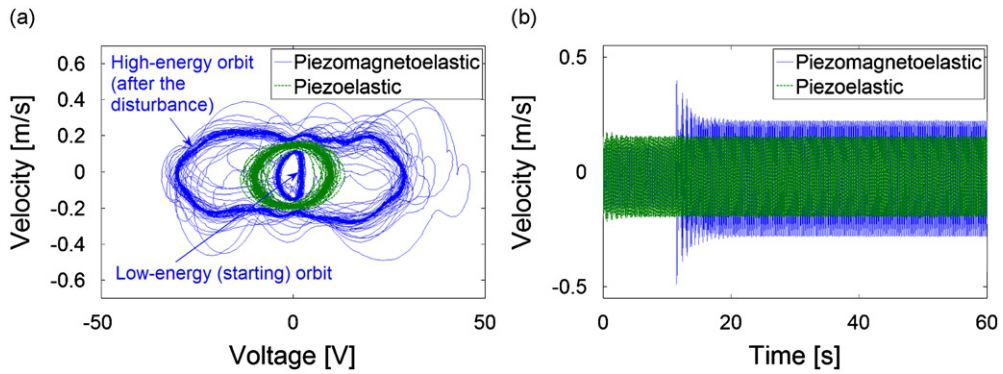


**Fig. 14.** (a) Comparison of the electromechanical trajectories for the piezomagnetoelastic and the piezoelectric configurations showing that the starting motion of the piezomagnetoelastic configuration is a small-amplitude limit-cycle until the disturbance at  $t=11$  s and (b) velocity histories of both configurations showing the instant of disturbance for the piezomagnetoelastic configuration (excitation: 0.5g at 6 Hz).

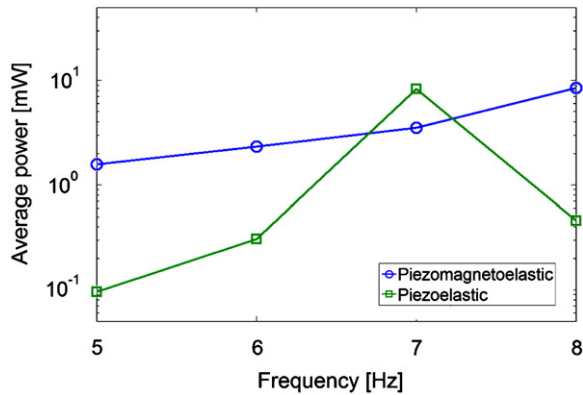


**Fig. 15.** Comparison of the average power outputs of the piezomagnetoelastic and the piezoelectric energy harvester configurations (rms acceleration input: 0.35g).

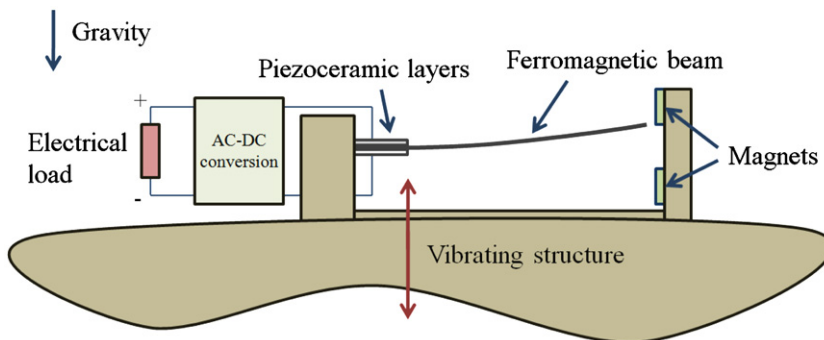


**Fig. 16.** Schematic of a piezomagnetoelastic energy harvester under vertical excitation.

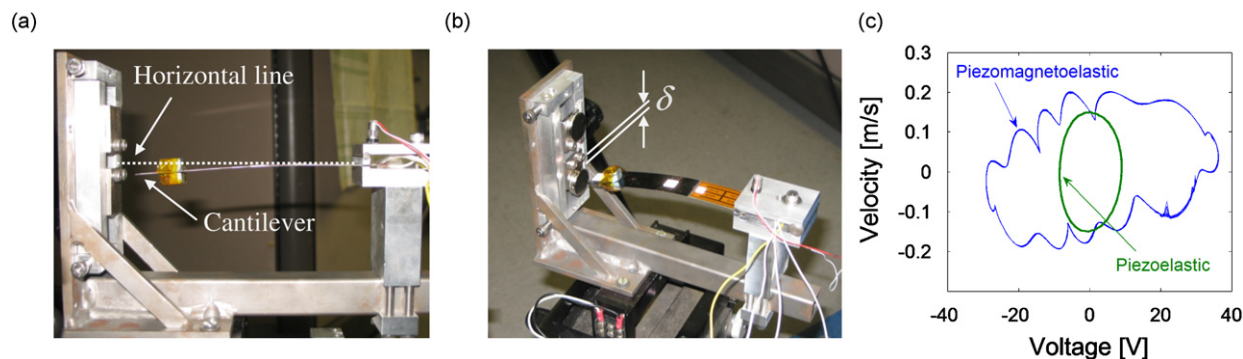


**Fig. 17.** (a) Static deflection of the piezoelectric beam due to gravity (in the absence of magnets), (b) piezomagnetoelastic configuration with the lower magnet moved downwards to balance the magnetic attraction and (c) comparison of the steady-state periodic orbits in the piezomagnetoelastic and piezoelectric configurations after the adjustment (for a vertical excitation amplitude of 0.5g at 5.5 Hz).

the lower magnet (i.e. the magnet that is at the ground side). As a result, the statically bistable beam can become statically monostable since the combined effect of the attraction of the lower magnet and the gravity overcomes the attraction of the upper magnet. From the dynamic point of view, the beam cannot escape the attraction of the lower magnet and the only possible steady-state response becomes small-amplitude oscillations around the lower magnet. A simple adjustment of the magnet spacing (to balance the transverse force resultant at the tip) can resolve the problem and the broadband phenomenon discussed herein can be preserved for vertical excitation as well (not necessarily for the exact same frequency range).

Fig. 17a shows the static deflection of the piezoelectric cantilever used in this work (in the absence of magnets) when it is located horizontally for vertical excitation. Since the sag of the flexible beam due to its weight is considerable, the piezomagnetoelastic configuration is no longer statically bistable when located horizontally. In order to reduce the attraction of the lower magnet, it is moved downwards by an empirical amount (Fig. 17b). Once the force balance at the tip of the beam is achieved, it is observed that similar large-amplitude limit-cycles can be obtained for the vertical excitation of the piezomagnetoelastic configuration as well. As in the case of horizontal excitation, limit-cycles of the piezomagnetoelastic configuration have much higher energy compared to those of the piezoelectric configuration (Fig. 17c).

## 5. Bistable magnetoelastic structure for other transduction mechanisms

High-energy orbits of the bistable magnetoelastic structure [28] can be employed for energy harvesting using other transduction mechanisms as well. Moreover, different transduction mechanisms can be combined to obtain hybrid devices utilizing the large-amplitude broadband response of the bistable configuration.

Fig. 18a describes the use of the bistable magnetoelastic structure for electrostatic energy harvesting. In this simple implementation, electrically isolated capacitor fingers are located on the faces of the elastic beam and they oscillate as the elastic beam vibrates in response to base excitation (the charge pump circuit in Fig. 18a is due to Roundy et al. [3] and Chiu and Tseng [42]). In electrostatic energy harvesting, the vibratory motion of the structure results in work done against the electrostatic forces between the capacitor fingers, which provides the harvested energy. Unlike in piezoelectric energy harvesting, a voltage input is required in electrostatic energy harvesting. One way of implementing the magnetoelastic structure for electromagnetic energy harvesting is shown in Fig. 18b. Extraction of electromagnetic power requires a relative motion between a magnet and a coil due to Faraday's law (e.g. moving magnet and stationary coil or moving coil and stationary magnet [1]). The configuration shown in Fig. 18b considers a moving coil cutting the magnetic field lines of the stationary magnets, yielding an alternating voltage output, which can then be rectified and regulated to charge a battery or a capacitor. More magnets can be included provided that they do not distort the magnetic field causing the bistability of the beam. The electromagnetic power output is proportional to the relative velocity between the coil and the magnet [1]. Magnetostrictive materials (e.g. Terfenol-D) deform when placed in a magnetic field and conversely they can induce changes in a magnetic field if strained mechanically [7,8]. A magnetostrictive material with a bias magnetic field can be located at the root of the cantilever (Fig. 18c). Large dynamic strains induced in the magnetostrictive layers under broadband harmonic excitation of the magnetoelastic configuration described herein can improve the power output considerably compared to conventional cantilevers used for magnetostrictive energy harvesting [7].

## 6. Summary and conclusions

Theoretical and experimental investigations of broadband high-energy orbits in a bistable piezomagnetoelastic energy harvester are presented along with a brief comparative study for the chaotic response. The lumped-parameter equations describing the system dynamics for the fundamental vibration mode successfully describe the broadband large-amplitude voltage response of the piezomagnetoelastic configuration. Electromechanical phase trajectories of the piezomagnetoelastic

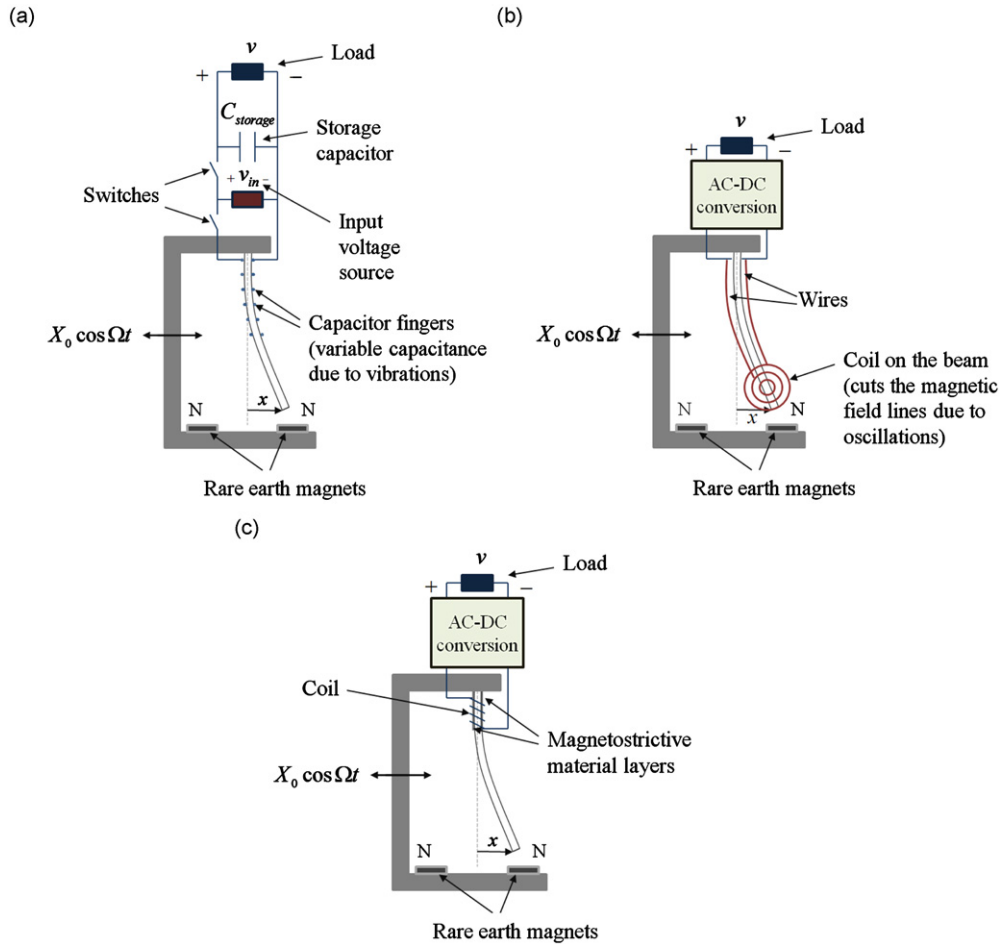


**Fig. 18.** (a) Electrostatic, (b) electromagnetic and (c) magnetostrictive energy harvesting using the bistable magnetoelastic structure.

and the piezoelectric configurations are compared theoretically and the substantial advantage of the former is observed at several frequencies. This observation is verified experimentally by showing that the piezomagnetoelastic configuration can generate an order of magnitude larger power compared to commonly employed piezoelectric configuration over a range of frequencies. The chaotic response of the piezomagnetoelastic configuration is also compared against the periodic response of the piezoelectric configuration for the same acceleration input. It is observed that the rms voltage output of the chaotic response in the piezomagnetoelastic configuration and that of the periodic response in the piezoelectric configuration can be very similar. In such a case, the periodic response of the conventional piezoelectric configuration is preferable from the signal processing standpoint (for designing an efficient energy harvesting circuit to charge a storage component). On the other hand, the periodic signal output obtained from the large-amplitude limit-cycle oscillations discussed herein can be processed with the existing nonlinear circuits for storage applications. However, a major parameter for attraction by the high-energy orbits is the excitation amplitude. For the non-optimized prototype discussed in this paper, 0.35g rms acceleration (with excitation frequencies less than 10 Hz) is sufficient for the 14.5-cm-long cantilever, yielding an average power output as high as 8.45 mW. Since vertical excitation is required in various applications, how to overcome the bias caused by the gravity is discussed experimentally. Utilization of high-energy orbits in the bistable structural configuration for electrostatic, electromagnetic and magnetostrictive transduction mechanisms is also summarized.

## Acknowledgements

The authors gratefully acknowledge the support from the U.S. Air Force Office of Scientific Research under the grants F9550-06-1-0326, "Energy Harvesting and Storage Systems for Future Air Force Vehicles", F9550-09-1-0625, "Simultaneous Vibration Suppression and Energy Harvesting" monitored by Dr. B.L. Lee and the support from the U.S. Department of Commerce, National Institute of Standards and Technology, Technology Innovation Program, Cooperative Agreement Number 70NANB9H9007, "Self-Powered Wireless Sensor Network for Structural Health Prognosis".

## References

- [1] P. Glynne-Jones, M.J. Tudor, S.P. Beeby, N.M. White, An electromagnetic, vibration-powered generator for intelligent sensor systems, *Sensors and Actuators A* 110 (2004) 344–349.
- [2] D. Arnold, Review of microscale magnetic power generation, *IEEE Transactions on Magnetics* 43 (2007) 3940–3951.
- [3] S. Roundy, P.K. Wright, J.M. Rabaey, A study of low level vibrations as a power source for wireless sensor nodes, *Computer Communications* 26 (2003) 1131–1144.
- [4] P. Mitcheson, P. Miao, B. Start, E. Yeatman, A. Holmes, T. Green, MEMS electrostatic micro-power generator for low frequency operation, *Sensors and Actuators A* 115 (2004) 523–529.
- [5] S. Roundy, P.K. Wright, A piezoelectric vibration based generator for wireless electronics, *Smart Materials and Structures* 13 (2004) 1131–1144.
- [6] A. Erturk, D.J. Inman, An experimentally validated bimorph cantilever model for piezoelectric energy harvesting from base excitations, *Smart Materials and Structures* 18 (2009) 025009.
- [7] L. Wang, F.G. Yuan, Vibration energy harvesting by magnetostrictive material, *Smart Materials and Structures* 17 (2008) 045009.
- [8] A. Adly, D. Davino, A. Giustiniani, C. Visone, Experimental tests of a magnetostrictive energy harvesting device towards its modeling, *Journal of Applied Physics* 107 (2010) 09A935.
- [9] H. Sodano, G. Park, D.J. Inman, A review of power harvesting from vibration using piezoelectric materials, *Shock and Vibration Digest* 36 (2004) 197–205.
- [10] S.R. Anton, H.A. Sodano, A review of power harvesting using piezoelectric materials (2003–2006), *Smart Materials and Structures* 16 (2007) R1–R21.
- [11] S. Priya, Advances in energy harvesting using low profile piezoelectric transducers, *Journal of Electroceramics* 19 (2007) 167–184.
- [12] K.A. Cook-Chennault, N. Thambi, A.M. Sastry, Powering MEMS portable devices—a review of non-regenerative and regenerative power supply systems with emphasis on piezoelectric energy harvesting systems, *Smart Materials and Structures* 17 (2008) 043001.
- [13] J.M. Renno, M.F. Daqaq, D.J. Inman, On the optimal energy harvesting from a vibration source, *Journal of Sound and Vibration* 320 (2009) 386–405.
- [14] N.G. Elvin, A.A. Elvin, A general equivalent circuit model for piezoelectric generators, *Journal of Intelligent Material Systems and Structures* 20 (2009) 3–9.
- [15] A.H. Nayfeh, D.T. Mook, *Nonlinear Oscillations*, John Wiley and Sons, New York, 1979.
- [16] J. Guckenheimer, P. Holmes, *Nonlinear Oscillations, Dynamical Systems, and Bifurcations of Vector Fields*, Springer-Verlag, New York, 1983.
- [17] S.G. Burrow, L.R. Clare, A. Carrella, D. Barton, Vibration energy harvesters with non-linear compliance, *Proceedings of SPIE* 6928 (2008) 692807.
- [18] B.P. Mann, N.D. Sims, Energy harvesting from the nonlinear oscillations of magnetic levitation, *Journal of Sound and Vibration* 319 (2009) 515–530.
- [19] R. Ramlan, M.J. Brennan, B.R. Mace, I. Kovacic, Potential benefits of a non-linear stiffness in an energy harvesting device, *Nonlinear Dynamics* 59 (2009) 545–558.
- [20] M.F. Daqaq, Response of uni-modal Duffing-type harvesters to random forced excitations, *Journal of Sound and Vibration* 329 (2010) 3621–3631.
- [21] S.C. Stanton, C.C. McGehee, B.P. Mann, Reversible hysteresis for broadband magnetopiezoelectric energy harvesting, *Applied Physics Letters* 96 (2010) 174103.
- [22] F. Cottone, H. Vocca, L. Gammaitoni, Nonlinear energy harvesting, *Physical Review Letters* 102 (2009) 080601.
- [23] L. Gammaitoni, I. Neri, H. Vocca, Nonlinear oscillators for vibration energy harvesting, *Applied Physics Letters* 94 (2009) 164102.
- [24] R. Benzi, A. Sutera, A. Vulpiani, The mechanism of stochastic resonance, *Journal of Physics A: Mathematical and General* 14 (1981) L453–L457.
- [25] C.R. McInnes, D.G. Gorman, M.P. Cartmell, Enhanced vibrational energy harvesting using nonlinear stochastic resonance, *Journal of Sound and Vibration* 318 (2008) 655–662.
- [26] S.C. Stanton, C.C. McGehee, B.P. Mann, Nonlinear dynamics for broadband energy harvesting: investigation of a bistable inertial generator, *Physica D* 239 (2010) 640–653.
- [27] A. Erturk, J. Hoffmann, D.J. Inman, A piezomagnetoelastic structure for broadband vibration energy harvesting, *Applied Physics Letters* 94 (2009) 254102.
- [28] F.C. Moon, P.J. Holmes, A magnetoelastic strange attractor, *Journal of Sound and Vibration* 65 (1979) 275–296.
- [29] T. Poston, O. Stewart, *Catastrophe Theory and Its Applications*, Pitman, London, 1979.
- [30] P. Holmes, A nonlinear oscillator with a strange attractor, *Philosophical Transactions of the Royal Society of London, Series A* 292 (1979) 419–449.
- [31] A. Triplett, D.D. Quinn, The effect of non-linear piezoelectric coupling on vibration-based energy harvesting, *Journal of Intelligent Material Systems and Structures* 20 (2009) 1959–1967.
- [32] S.C. Stanton, A. Erturk, B.P. Mann, D.J. Inman, Nonlinear piezoelectricity in electroelastic energy harvesters: modeling and experimental identification, *Journal of Applied Physics* 108 (2010) 074903.
- [33] S.C. Stanton, B.P. Mann, Nonlinear electromechanical dynamics of piezoelectric inertial generators: modeling, analysis, and experiment, *Nonlinear Dynamics*, in review.
- [34] Standards Committee of the IEEE Ultrasonics, Ferroelectrics, and Frequency Control Society, IEEE Standard on Piezoelectricity, IEEE, New York.
- [35] G.K. Ottman, H.F. Hofmann, G.A. Lesieutre, Optimized piezoelectric energy harvesting circuit using step-down converter in discontinuous conduction mode, *IEEE Transactions on Power Electronics* 18 (2003) 696–703.
- [36] M.J. Guan, W.H. Liao, On the efficiencies of piezoelectric energy harvesting circuits towards storage device voltages, *Smart Materials and Structures* 16 (2007) 498–505.
- [37] E. Lefeuvre, D. Audigier, C. Richard, D. Guyomar, Buck-boost converter for sensorless power optimization of piezoelectric energy harvester, *IEEE Transactions on Power Electronics* 22 (2007) 2018–2025.
- [38] Y.C. Shu, I.C. Lien, W.J. Wu, An improved analysis of the sshi interface in piezoelectric energy harvesting, *Smart Materials and Structures* 16 (2007) 2253–2264.
- [39] W.J. Wu, A.M. Wickenheiser, T. Reissman, E. Garcia, Modeling and experimental verification of synchronized discharging techniques for boosting power harvesting from piezoelectric transducers, *Smart Materials and Structures* 18 (2009) 055012.
- [40] N. Kong, D.S. Ha, A. Erturk, D.J. Inman, Resistive impedance matching circuit for piezoelectric energy harvesting, *Journal of Intelligent Material Systems and Structures* 21, doi:10.1177/1045389x09357971, in press.
- [41] G. Litak, M.I. Friswell, S. Adhikari, Magnetoelastic energy harvesting driven by random excitations, *Applied Physics Letters* 96 (2010) 214103.
- [42] Y. Chiu, V.F.G. Tseng, A capacitive vibration-to-electricity energy converter with integrated mechanical switches, *Journal of Micromechanical and Microengineering* 18 (2008) 104004.